Reprinted from

JAPANESE JOURNAL OF
APPLIED
PHYSICS

REGULAR PAPER

Simulation of Thick Gated Silicon Drift X-ray Detector Operated by a Single High-Voltage Source

Hideharu Matsuura

Jpn. J. Appl. Phys. **52** (2013) 024301

Japanese Journal of Applied Physics **52** (2013) 024301 **REGULAR PAPER**
http://dx.doi.org/**10.7567/JJAP.52.024301**

Simulation of Thick Gated Silicon Drift X-ray Detector Operated by a Single High-Voltage Source

Hideharu Matsuura*

Department of Electric and Electronic Engineering, Osaka Electro-Communication University, Neyagawa, Osaka 572-8530, Japan
E-mail: matsuura@isc.osakac.ac.jp

Received July 10, 2012; revised November 2, 2012; accepted November 14, 2012; published online January 16, 2013

High-resolution X-ray detectors can be used to detect traces of hazardous or radioactive elements in food, soil, and the human body by measuring the energies and counts of emitted X-ray fluorescence photons. We have simulated the electric potential distributions in gated silicon drift detectors (GSDDs) with an active area of 18 mm^2 and a Si thickness between 0.625 and 1.5 mm. A GSDD gate pattern was designed for each Si thickness and for various oxide charge densities in the SiO_2 passivating layer near the SiO_2/Si interface. The simulated GSDDs required approximately half the reverse bias voltage required by Si pin detectors. Our detector design could improve the absorption of Cd or Cs X-ray fluorescence photons and would reduce the cost of X-ray detection systems. © 2013 The Japan Society of Applied Physics

1. Introduction

The relationship between disease development and traces of hazardous or radioactive elements in body organs and tissues can be investigated by detecting the X-ray fluorescence photons emitted by these elements, particularly during radiographic examinations or computed tomography. Various types of X-ray detectors, such as Si pin detectors and silicon drift detectors (SDDs),[1–29] are used to measure the energy and photon count of an X-ray fluorescence photon. A pin diode can be used for collecting charge carriers, whose number is proportional to the energy of an X-ray photon. In X-ray fluorescence spectroscopy, the capacitance of a pin detector increases with the active area of the detector, which degrades its performance. The capacitance is lower in an SDD;[1] however, because the anode (n-layer), which is on one surface of the n^--type Si substrate (n^- or i-layer), is smaller than the pin diode; an SDD also has a large entrance window layer, which is the cathode or p-layer, on the opposite surface. The anode is surrounded by multiple p-type rings (p-rings), to which bias voltage is applied. The resulting electric field makes the electrons flow smoothly toward the anode. To form a sufficiently strong electric field in a commercial SDD, the p-rings are electrically coupled using expensive built-in metal–oxide–semiconductor field-effect transistors (MOSFETs) or implanted resistors. With the aim of realizing low-cost detectors, we have designed several simple SDDs without MOSFETs or implanted resistors.[30–35]

To detect traces of hazardous or radioactive elements in food, soil, and human bodies, the absorption of Cd (23.1 keV) and Cs X-ray fluorescence photons (30.8 keV) by SDDs must be increased. However, the thickness of the Si substrates in commercial SDDs is approximately 0.3 mm; thus, the absorbed fractions of Cd and Cs X-ray fluorescence photons are 19.1 and 7.7%, respectively. In contrast, for a 1.5-mm-thick Si substrate, the absorbed fractions increase to 65.4 and 33.1%, respectively.

To produce inexpensive X-ray fluorescence instruments, it is also necessary to avoid high-energy X-ray generators. For example, the X-ray photon excitation energy required to produce the K-line X-ray fluorescence photons for U is greater than 98.4 keV. Therefore, we propose that the X-ray fluorescence photons of hazardous elements, such as As, Hg, and Pb, and radioactive elements, such as Sr, U, and Pu, could be detected at lower energies (10.5, 10.0, 10.6, 14.1, 13.6, and 14.3 keV, respectively).

Cadmium telluride (CdTe) X-ray detectors can detect X-ray photons with energies greater than 25 keV, whereas Si X-ray detectors can detect photons with energies less than 25 keV. To realize detection of X-ray fluorescence photons with energies between 10 and 30 keV, thicker-Si X-ray detectors have been investigated.[36–38]

In addition, in order to use X-ray fluorescence spectrometers on site, the detectors must be portable. Therefore, we have investigated a compact, portable Peltier cooling mechanism for thick-Si X-ray detectors with a simple structure. We previously reported prototype gated silicon drift detectors (GSDDs) that contained 0.625-mm-thick Si substrates with an effective active area of 18 mm^2, and the simulation results for a 1.5-mm-thick GSDD with an effective active area of 3 mm^2.[35] In the present study, we used a device simulator to design gate patterns for GSDDs that contained 0.625-, 1.0-, and 1.5-mm-thick Si substrates with an active area of 18 mm^2.

2. Structure of the Gated Silicon Drift Detector

To operate an X-ray detector with a thick Si substrate at a moderate reverse bias, the resistivity of n^- Si substrates should be greater than 2 kΩ·cm for commercial SDDs.[34,35] However, large hole currents flow between the cathode and some of the p-rings in SDDs with high-resistivity Si substrates, because of the large difference in voltage between the cathode and the p-rings.[34,35]

Figure 1 shows a schematic cross section of a cylindrical GSDD with several ring-shaped gates and one p-ring that does not have MOSFETs or implanted resistors.[32,33] Because the metal gates are formed on the passivating oxide layer (SiO_2) during the metallization of the anode and the p-ring, there are no extra fabrication processes required to form the gates. As a result, the fabrication of GSDDs is much simpler than that of commercial SDDs. Moreover, the same high reverse bias can be applied to the cathode, the p-ring, and all the gates, which means that GSDDs require only one high-voltage source. This design greatly reduces the cost of the X-ray detection system.

3. Device Simulation Results and Discussion

3.1 0.625-mm-thick GSDD

The device simulations were carried out using ATLAS

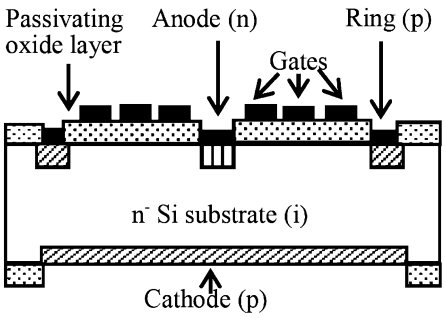

Fig. 1. Schematic cross section of a cylindrical GSDD structure with one p-ring and several gates. The same negative voltage was applied to the cathode, the p-ring, and all the gates.

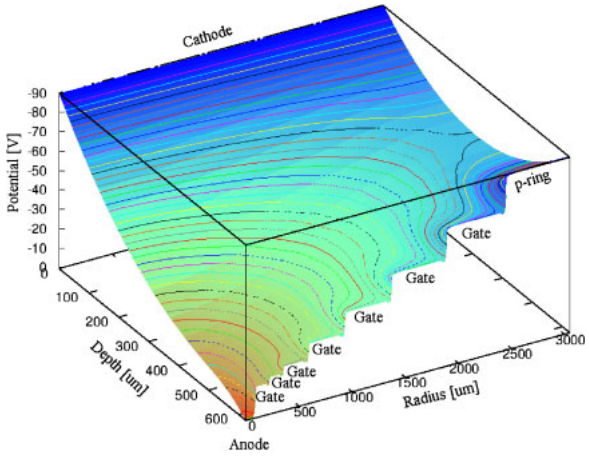

Fig. 2. (Color online) Simulated electric potential distribution in the GSDD Si substrate for gate pattern A in a 0.625-mm-thick Si substrate with a resistivity of 10 kΩ·cm. A reverse bias voltage of −90 V was applied to the cathode, p-ring, and seven gates. Q_F was assumed to be 3×10^{10} cm^{-2}.

software (Silvaco). In the simulation, the thickness and resistivity of the n^- Si substrate were 0.625 mm and 10 kΩ·cm, respectively. The radius of the anode was 0.055 mm, the inner radius of the p-ring was 2.455, and the outer radius was 3.05 mm. Seven gates were used. The widths of the seven gates, from the innermost to the outermost, were 0.1, 0.1, 0.19, 0.29, 0.39, 0.47, and 0.51 mm. For gate pattern A, the gap between the anode and the innermost gate was 0.04 mm, and the gaps between the innermost and second gates, and between the second and third gates, were both 0.03 mm. The other gaps between the gates and the gap between the outermost gate and the p-ring were all 0.05 mm.

The acceptor densities of the cathode and the p-ring were 1×10^{18} cm^{-3}, and the donor density of the anode was 1×10^{19} cm^{-3}. The depths of the cathode, p-ring, and anode were all 1 μm. The thickness of the SiO_2 layer was 0.75 μm, and the positive fixed oxide charge sheet density (Q_F) in SiO_2 near the SiO_2/Si interface was varied. The same reverse bias voltage (V_R) was applied to the cathode, the p-ring, and all the gates.

Figure 2 shows the simulated electric potential distribution in the GSDD Si substrate at V_R of −90 V with Q_F of 3×10^{10} cm^{-2}, which has been reported for the present fabrication process.[39] The voltage midway between the p-ring and the cathode was −62 V, and the electric field along the electric potential valley was strong enough to make all the electrons produced by an X-ray photon smoothly flow to the anode. Therefore, the electrons produced within the radius of the inner edge of the p-ring can be directed to the anode, indicating that the effective active area is approximately 18 mm^2.

Q_F depends strongly on how the SiO_2 layers are formed. The electric potential distributions for various Q_F values were simulated, because the gate widths and the gaps should allow the detectors to function satisfactorily even when Q_F is changed by the fabrication process. An adequate electric potential distribution was obtained, when Q_F was 1×10^{12} cm^{-2}.

The drift time of electrons increases the further they are produced from the anode. When the electrons travel far from the anode, positive charges are induced by the drifting electrons at the p-ring, gates, and cathode, but not at the anode, indicating that the induced current does not appear at the anode. When the electrons drift between the anode and the innermost gate, the induced current signal is detected at the anode. Therefore, the signal rise time is short even in GSDDs with a large entrance window.

Previously, an energy resolution of 145 eV at 5.9 keV was obtained from a ^{55}Fe source at −38 °C.[35] The effective active area of the detector was found to be approximately 18 mm^2 by irradiating X-ray photons through a 0.1-mm-diameter pinhole, which is in good agreement with our simulation.

3.2 1-mm-thick GSDD

Because V_R of −160 V was required in 1-mm-thick GSDDs, the thickness of SiO_2 was changed from 0.75 to 1.5 μm to avoid SiO_2 breakdown caused by the high electric field.

Figure 3(a) shows the simulated electric potential distribution in the 1-mm-thick Si GSDD substrate for gate pattern A at V_R of −160 V with Q_F of 3×10^{10} cm^{-2}. A flat area in the electric potential was visible between 0.1 and 0.3 mm from the anode toward the cathode, indicating that the electron–hole pairs produced by an X-ray photon could recombine easily in this area.

Therefore, the gate design was changed to ensure an adequate electric potential distribution. For gate pattern B, the gaps between the innermost and second gates and between the second and third gates were increased from 0.03 to 0.09 mm, and the gap between the third and fourth gates was also increased from 0.05 to 0.07 mm, because the voltage drops between the innermost and second gates and between the second and third gates were too small in gate pattern A. The gaps between the sixth and outermost gates and between the outermost gate and the p-ring were reduced from 0.05 to 0.03 mm, because the voltage drops at these gaps were large. In addition, the widths of the third, fourth, fifth, sixth, and outermost gates were changed to 0.17, 0.27, 0.37, 0.45, and 0.49 mm, respectively.

Figure 3(b) shows the simulated electric potential distribution in a 1-mm-thick Si substrate for the GSDD with gate pattern B at V_R of −160 V and Q_F of 3×10^{10} cm^{-2}. The flat area in the electric potential disappeared and the voltage midway between the p-ring and the cathode was −73 V. The electric field along the electric potential valley

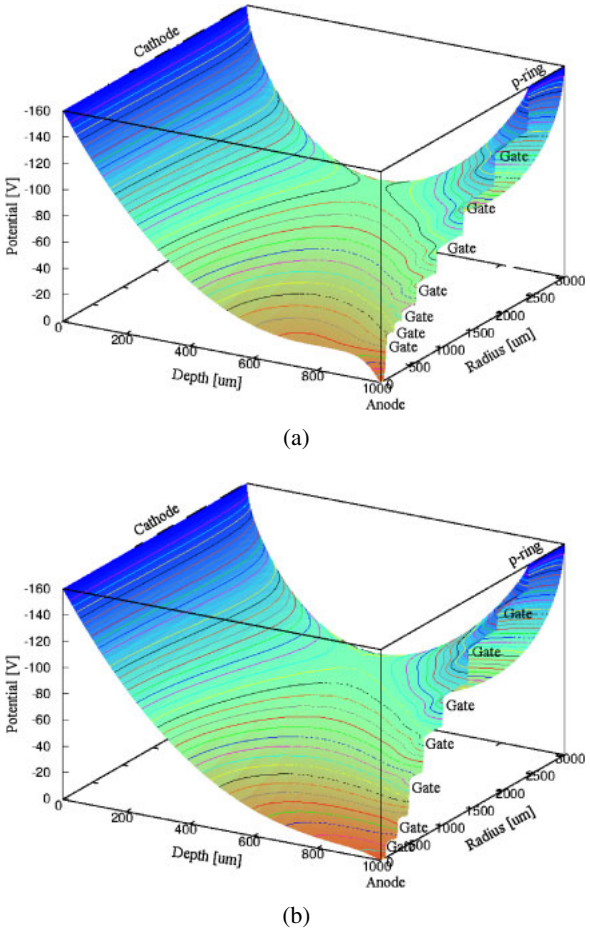

Fig. 3. (Color online) Simulated electric potential distributions in 1-mm-thick GSDD Si substrates with resistivity of 10 kΩ·cm for (a) gate pattern A and (b) gate pattern B. A reverse bias voltage of −160 V was applied to the cathode, p-ring, and seven gates. Q_F was assumed to be 3×10^{10} cm^{-2}.

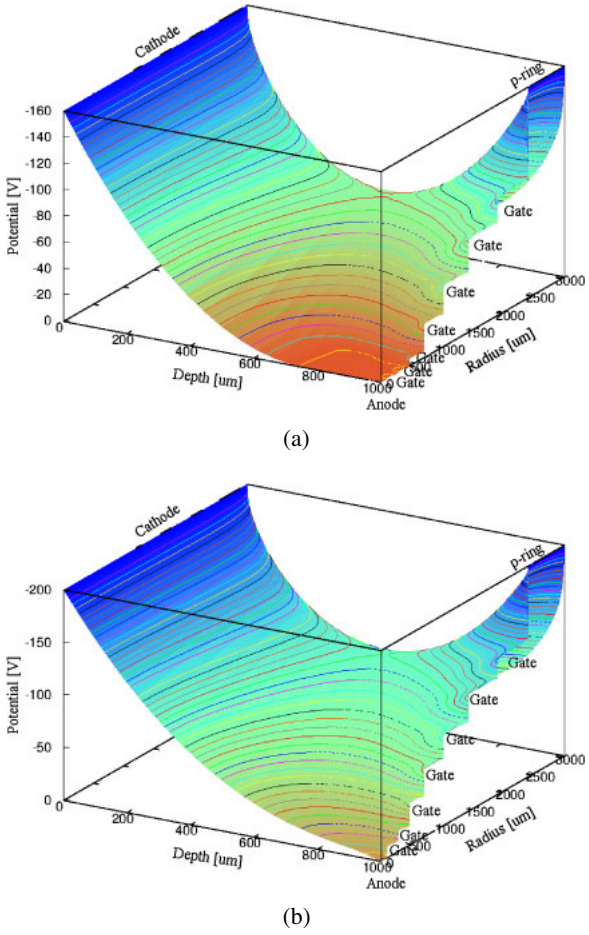

Fig. 4. (Color online) Simulated electric potential distributions in 1-mm-thick GSDD Si substrates with gate pattern B and a resistivity of 10 kΩ·cm for Q_F of 1×10^{12} cm^{-2}. Reverse bias voltages of (a) −160 and (b) −200 V were applied to the cathode, p-ring, and seven gates.

was strong enough to make all the electrons produced by the X-ray photons flow smoothly to the anode.

Figures 4(a) and 4(b) show the simulated electric potential distributions in the 1-mm-thick Si GSDD substrate for gate pattern B with Q_F of 1×10^{12} cm^{-2} at V_R values of −160 and −200 V, respectively. At −160 V, the voltage under the innermost gate was nearly 0 V, and the electric field for a large area near the anode was 0 V/cm, which indicates that electron–hole pairs produced by an X-ray photon in this area would recombine easily. Figure 4(b) shows that V_R of −200 V was required to obtain an adequate electric potential distribution in gate pattern B for Q_F of 1×10^{12} cm^{-2}. Therefore, the 1-mm-thick GSDD with gate pattern B would work well if V_R was changed slightly.

For a Si pin diode with a 1-mm-thick Si substrate and a resistivity of 10 kΩ·cm, a reverse bias of approximately −300 V is required to deplete the whole Si layer. For the GSDD, a reverse bias of only −160 V was required.

3.3 1.5-mm-thick GSDD

Figure 5(a) shows the simulated electric potential distribution in the 1.5-mm-thick Si GSDD substrate for gate pattern B at V_R of −320 V with Q_F of 3×10^{10} cm^{-2}. The thickness of the SiO_2 layer was 1.5 µm. For gate pattern B, the voltage drop between the anode and the innermost gate was very large, which produced a flat area in the electric potential between 0.1 and 0.7 mm from the anode to the cathode. In this area, electron–hole pairs produced by an X-ray photon would recombine easily and would not be detected.

For gate pattern C, the gap between the anode and the innermost gate was 0.16 mm, and the gap between the innermost and second gates was 0.11 mm. In addition, the widths of the innermost, second, third, fourth, fifth, sixth, and outermost gates were changed to 0.15, 0.25, 0.25, 0.28, 0.28, 0.3, and 0.3 mm, respectively.

Figure 5(b) shows the simulated electric potential distribution in the 1.5-mm-thick Si GSDD substrate for gate pattern C at V_R of −320 V with Q_F of 3×10^{10} cm^{-2}. In the electric potential distribution, the voltage midway between the p-ring and the cathode was −110 V, which was larger than that in the 0.625-mm-thick GSDD, although the voltage drop between the midway point and the anode appeared to be too small. Therefore, the electric field along the electric potential valley was strong enough to make all the electrons produced by the X-ray photons flow smoothly to the anode.

Figures 6(a) and 6(b) show the simulated electric potential distributions in the 1.5-mm-thick Si GSDD substrates for gate pattern C with Q_F of 1×10^{12} cm^{-2} and V_R values of −320 and −400 V, respectively. At −320 V, the voltage

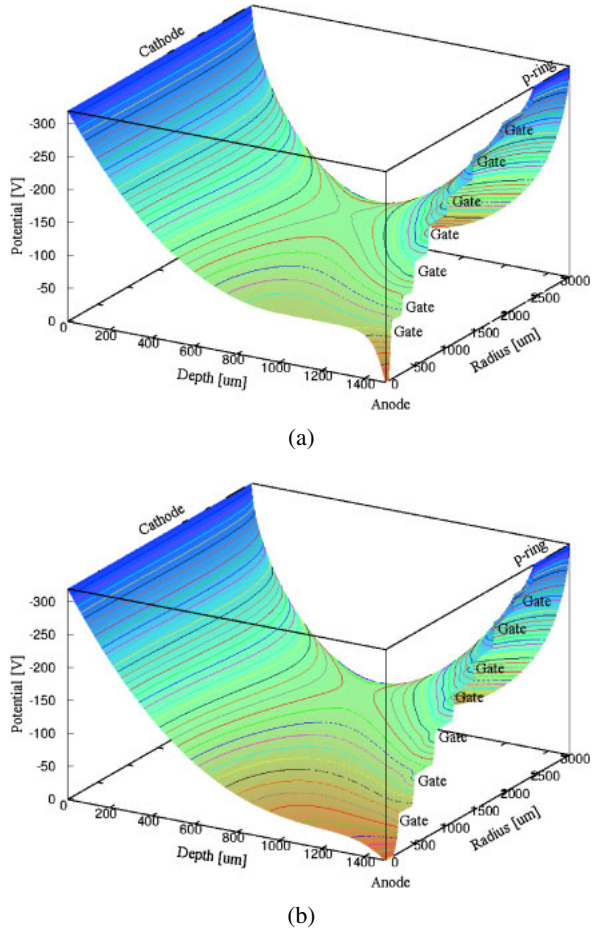

Fig. 5. (Color online) Simulated electric potential distributions in 1.5-mm-thick Si GSDD substrates with a resistivity of 10 kΩ·cm for (a) gate pattern B and (b) gate pattern C. A reverse bias voltage of −320 V was applied to the cathode, p-ring, and seven gates. Q_F was assumed to be 3×10^{10} cm^{-2}.

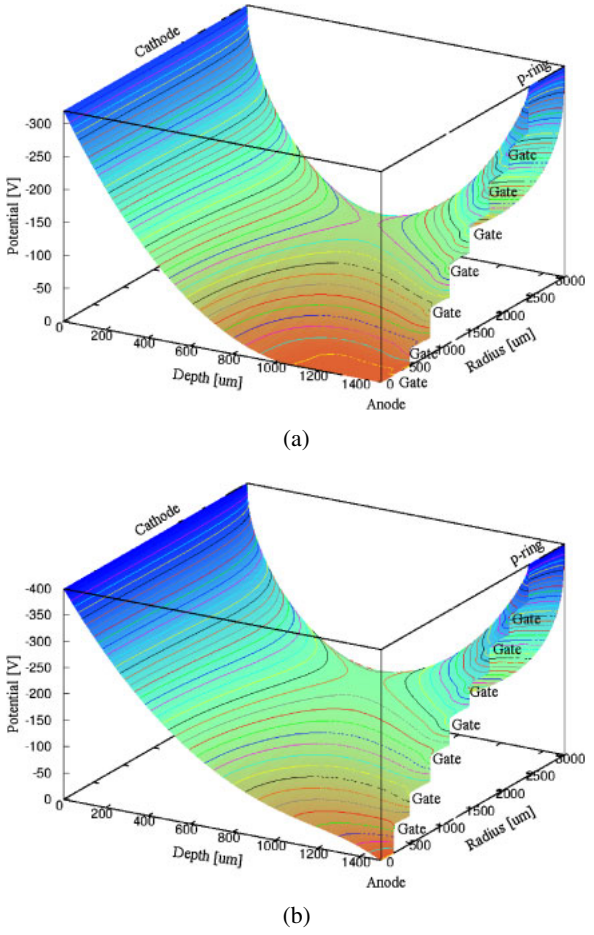

Fig. 6. (Color online) Simulated electric potential distributions in 1.5-mm-thick Si GSDD substrates for gate pattern C with a resistivity of 10 kΩ·cm and Q_F of 1×10^{12} cm^{-2}. Reverse bias voltages of (a) −320 and (b) −400 V were applied to the cathode, p-ring, and seven gates.

under the innermost gate was nearly 0 V, and a large area of the electric field near the anode was 0 V/cm. However, at −400 V the electric field along the electric potential valley was strong enough to make all the electrons produced by the X-ray photons flow smoothly to the anode. Therefore, the GSDDs fabricated with this design should work well if the V_R is changed slightly.

For a Si pin diode with a 1.5-mm-thick Si substrate with a resistivity of 10 kΩ·cm, a reverse bias of approximately −680 V is required to deplete the whole Si layer. However, for the GSDD, a reverse bias of less than −400 V was required.

4. Conclusions

Thick Si X-ray detectors with a simple structure were investigated in order to develop inexpensive, portable X-ray detectors that can detect and accurately count X-ray fluorescence photons with energies between 10 and 30 keV. A device simulation of GSDDs with a 1.5-mm-thick Si substrate indicated that they should work well when they are produced using current fabrication processes. Moreover, the operating high reverse biases in the GSDDs were predicted to be half those in the pin diodes. Our simulation results indicate that the cost of portable X-ray fluorescence instruments can be significantly reduced.

Acknowledgments

The author thanks R. Okada, S. Kitanoya, and S. Nishikawa of our laboratory, Dr. D. Hullinger and Dr. K. W. Decker of MOXTEK, Inc., and Dr. K. Taniguchi and Dr. T. Utaka of Techno X Co., Ltd., for helpful discussions.

1) E. Gatti and P. Rehak: Nucl. Instrum. Methods **225** (1984) 608.
2) P. Rehak, E. Gatti, A. Longoni, M. Sampietro, P. Holl, G. Lutz, J. Kemmer, U. Prechtel, and T. Ziemann: IEEE Trans. Nucl. Sci. **36** (1989) 203.
3) W. Chen, H. Kraner, Z. Li, P. Rehak, E. Gatti, A. Longoni, M. Sampietro, P. Holl, J. Kemmer, U. Faschingbauer, B. Schmitt, A. Wörner, and J. P. Wurm: IEEE Trans. Nucl. Sci. **39** (1992) 619.
4) E. A. Hijzen, E. M. Schooneveld, C. W. E. van Eijk, and R. W. Hollander: Nucl. Instrum. Methods Phys. Res., Sect. A **335** (1993) 271.
5) G. Bertuccio and A. Pullia: IEEE Trans. Nucl. Sci. **41** (1994) 1704.
6) E. Pinotti, A. Longoni, M. Gambelli, L. Strüder, P. Lechner, C. V. Zanthier, and H. Kraner: IEEE Trans. Nucl. Sci. **42** (1995) 12.
7) G. Gramegna, F. Corsi, D. De Venuto, C. Marzocca, A. Vacchi, V. Manzari, F. Navach, S. Beolé, G. Casse, P. Giubellino, L. Riccati, and P. Burger: IEEE Trans. Nucl. Sci. **42** (1995) 1497.
8) P. Lechner, S. Eckbauer, R. Hartmann, S. Krisch, D. Hauff, R. Richter, H. Soltau, L. Strüder, C. Fiorini, E. Gatti, A. Longoni, and M. Sampietro: Nucl. Instrum. Methods Phys. Res., Sect. A **377** (1996) 346.
9) A. Castoldi, P. Rehak, and P. Holl: Nucl. Instrum. Methods Phys. Res., Sect. A **377** (1996) 375.
10) J. S. Iwanczyk, B. E. Patt, J. Segal, J. Plummer, G. Vilkelis, B. Hedman,

K. O. Hodgson, A. D. Cox, L. Rehn, and J. Metz: Nucl. Instrum. Methods Phys. Res., Sect. A **380** (1996) 288.
11) Ch. Gauthier, J. Goulon, E. Moguiline, A. Rogalev, P. Lechner, L. Strüder, C. Fiorini, A. Longoni, M. Sampietro, H. Besch, R. Pfitzner, H. Schenk, U. Tafelmeier, A. Walenta, K. Misiakos, S. Kavadias, and D. Loukas: Nucl. Instrum. Methods Phys. Res., Sect. A **382** (1996) 524.
12) R. Hartmann, L. Strüder, J. Kemmer, P. Lechner, O. Fries, E. Lorenz, and R. Mirzoyan: Nucl. Instrum. Methods Phys. Res., Sect. A **387** (1997) 250.
13) C. Fiorini, J. Kemmer, P. Lechner, K. Kromer, M. Rohde, and T. Schülein: Rev. Sci. Instrum. **68** (1997) 2461.
14) H. Matsuura and K. Nishida: Jpn. J. Appl. Phys. **37** (1998) L115.
15) A. Rashevsky, V. Bonvicini, A. Vacchi, N. Zampa, P. Burger, S. Beole, M. Idzik, C. Petta, and N. Randazzo: Nucl. Instrum. Methods Phys. Res., Sect. A **409** (1998) 210.
16) J. Šonský, H. Valk, C. P. Allier, R. W. Hollander, C. W. E. van Eijk, and P. M. Sarro: IEEE Trans. Nucl. Sci. **46** (1999) 53.
17) J. S. Iwanczyk, B. E. Patt, C. R. Tull, J. D. Segal, C. J. Kenney, J. Bradley, B. Hedman, and K. O. Hodgson: IEEE Trans. Nucl. Sci. **46** (1999) 284.
18) H. Matsuura, K. Akatani, M. Ueda, K. Segawa, H. Tomozawa, K. Nishida, and K. Taniguchi: Jpn. J. Appl. Phys. **38** (1999) L1015.
19) L. Strüder, N. Meidinger, D. Stotter, J. Kemmer, P. Lechner, P. Leutenegger, H. Soltau, F. Eggert, M. Rohde, and T. Schulein: Microsc. Microanal. **4** (1998) 622.
20) V. Bonvicini, L. Busso, P. Giubellino, A. Gregorio, M. Idzik, A. Kolojvari, L. M. Montano, D. Nouais, C. Petta, A. Rashevsky, N. Randazzo, S. Reito, F. Tosello, A. Vacchi, L. Vinogradov, and N. Zampa: Nucl. Instrum. Methods Phys. Res., Sect. A **439** (2000) 476.
21) K. Hansen and L. Tröger: IEEE Trans. Nucl. Sci. **47** (2000) 2748.
22) C. Fiorini, A. Longoni, F. Perotti, C. Labanti, E. Rossi, P. Lechner, H. Soltau, and L. Strüder: IEEE Trans. Nucl. Sci. **49** (2002) 995.
23) T. Eggert, O. Boslau, P. Goldstrass, and J. Kemmer: X-ray Spectrom. **33** (2004) 246.
24) P. Lechner, A. Pahlke, and H. Soltau: X-ray Spectrom. **33** (2004) 256.
25) W. Metzger, J. Engdahl, W. Rossner, O. Boslau, and J. Kemmer: IEEE Trans. Nucl. Sci. **51** (2004) 1631.
26) J. Kemmer, F. Wiest, A. Pahlke, O. Boslau, P. Goldstrass, T. Eggert, M. Schindler, and I. Eisele: Nucl. Instrum. Methods Phys. Res., Sect. A **544** (2005) 612.
27) G. Zampa, A. Rashevsky, and A. Vacchi: IEEE Trans. Nucl. Sci. **56** (2009) 832.
28) G. A. Carini, W. Chen, G. De Geronimo, J. A. Gaskin, J. W. Keister, Z. Li, B. D. Ramsey, P. Rehak, and D. P. Siddons: IEEE Trans. Nucl. Sci. **56** (2009) 2843.
29) G. Zampa, R. Campana, M. Feroci, A. Vacchi, V. Bonvicini, E. D. Monte, Y. Evangelista, F. Fuschino, C. Labanti, M. Marisaldi, F. Muleri, L. Pacciani, M. Rapisarda, A. Rashevsky, A. Rubini, P. Soffitta, N. Zampa, G. Baldazzi, E. Costa, I. Donnarumma, M. Grassi, F. Lazzarotto, P. Malcovati, M. Mastropietro, E. Morelli, and L. Picolli: Nucl. Instrum. Methods Phys. Res., Sect. A **633** (2011) 15.
30) H. Matsuura, K. Taniguchi, and T. Utaka: Japan Patent Application No. 2006-336727 (2006); H. Matsuura, K. Taniguchi, and T. Utaka: Japan Patent Publication No. 2008-153256 (2008).
31) H. Matsuura, K. Taniguchi, and T. Utaka: Japan Patent Application No. 2007-098037 (2007); H. Matsuura, K. Taniguchi, and T. Utaka: Japan Patent Publication No. 2008-258348 (2008).
32) H. Matsuura: Japan Patent Application No. 2009-157627 (2009); H. Matsuura: Japan Patent Publication No. 2011-014718 (2011).
33) D. Hullinger, H. Matsuura, K. Taniguchi, and T. Utaka: US Patent 8, 314, 468 (2012).
34) H. Matsuura, M. Takahashi, K. Kohara, K. Yamamoto, T. Maeda, and Y. Kagawa: Denshi Joho Tsushin Gakkai Ronbunshi C **J93-C** (2010) 303 [in Japanese].
35) H. Matsuura, D. Hullinger, R. Okada, S. Kitanoya, S. Nishikawa, and K. Decker: Key Eng. Mater. **495** (2012) 294.
36) C. R. Tull, J. S. Iwanczyk, B. E. Patt, S. Barkan, and L. Feng: IEEE Trans. Nucl. Sci. **51** (2004) 1803.
37) S. Parker, C. Kenney, and J. Segal: Nucl. Instrum. Methods Phys. Res., Sect. A **395** (1997) 328.
38) M. Christophersen and B. F. Phlips: presented at IEEE Nuclear Science Symp., 2008.
39) B. L. Anderson and R. L. Anderson: *Fundamentals of Semiconductor Devices* (McGraw-Hill, New York, 2005) p. 497.